Inriamericwaves
Report of activities - March-May/16

Joao Guilherme Caldas Steinstraesser
José Galaz

May 27, 2016

Contents

1 Introduction

This report presents the initial work developed in the project, between march and may. On the long term, the objective of this project is to be able to simulate the propagation of water waves using a numerical model, understood as an algorithm or computer program, that can capture the physics associated to all different scales and phenomena, from the ocean to the shore and also including the intrinsic variability in the generation process of water waves. The methodology that has been chosen for this goal is to couple different models that are currently known as the best representation for the physics associated to each scale, by means of developing proper boundary conditions. Hence the interest of the study is split in two parts that are being run in parallel: first to get some familiarity with the equations and the physics we want to represent, and second, to get introduced to the study of the boundary conditions that will serve as communicators between our models.

The work that has been done from March to May has focused mainly on the study and implementation of nonlinear dispersive models for wave propagation: the KdV, BBM and Serre equations. In sections 2 to 4, we describe each one of these models, the theoretical study performed (for example, a scale analysis for the KdV equation) and the proposed discretizations for their computational resolution, using splitting schemes combining finite volume and spectral or finite difference methods. Some examples are presented to illustrate the numerical results and show the problems that must be corrected in the schemes.

Then, in section 5 we move to the other topic of interest which is the study of Transparent Boundary Conditions (TBC's). There, we describe a first approach and then proceed with the study of simple approximations to the TBC's in the case of the KdV equation.

1.1 Motivation example

In this section we show the importance of boundary conditions when modeling water waves propagation for the particular case of tsunami waves, using the free open source software GeoClaw [5] developed in the University of Washington, which uses a well-balanced shock capturing finite volume scheme with variable Adaptive Mesh Refinement (AMR) for the space discretization.

The simulation corresponds to the tsunami that struck the coast of Chile the year 2010 and two different domains have been chosen such that one is the extension of the other from the left boundary. Both domains, with their respective bathymetry and topography distribution, are shown in figure 1, and each domain is defined in geographic latitude and longitude coordinates

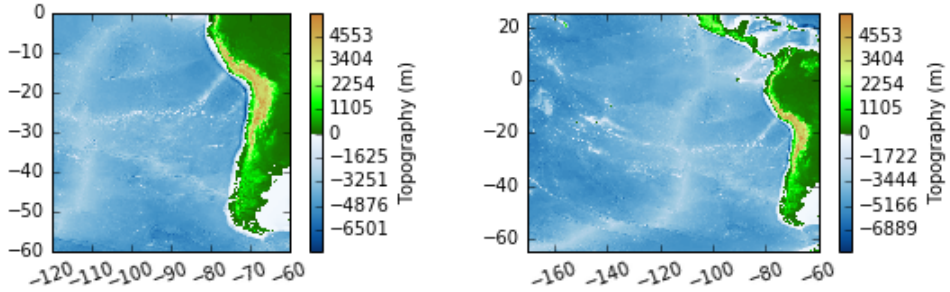

Figure 1: Topography and Bathymetry for domains Ω_1 and Ω_2 used in the simulations

Table 1: My caption

Lat (degrees)	-72.668
Lon (degrees)	-35.826
Length (km)	450
Width (km)	100
Strike (degrees)	16
Depth (km)	35
Slip (m)	15
Rake (degrees)	104
Dip (degrees)	14

by $\Omega_1 = [-120, -60] \times [-60, 0]$ and $\Omega_2 = [-170, -60] \times [-60, 0]$. Neumann boundary conditions are used for both domains, and the idea is to compare the values on the left boundary of Ω_1 with respect to those obtained there with Ω_2.

The initial conditions are defined as zero velocity and the deformation for the water free surface shown in figure 2 is the same as the seafloor deformation calculated by the dislocation model of Okada [9], using the fault parameters listed in table 1 proposed by the USGS for this case. The grid resolution is chosen as $\Delta x = \Delta y = 0.5$ degrees and the model is forced to not to use grid refinement.

Figures 3, 4, and 5 show the results of the simulations using Ω_1 and Ω_2 and the differences between Ω_1 and Ω_2 for the values of the free surface when the wave meets and leaves the boundary. From the values of the differences we can see that inside the domain there is some errors far from the boundaries that can be explained by both output interpolation of the software GeoClaw and the differences in fluxes at the boundaries of the patches that GeoClaw uses for managing the AMR, even when imposing fixed grids in the simulation. However it is possible to observe that the most important differences

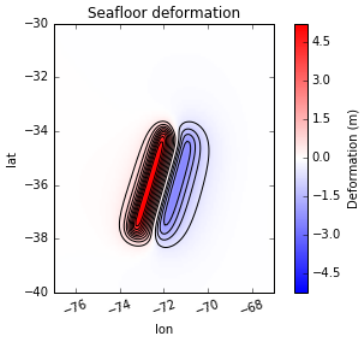

Figure 2: Deformation used for both the seafloor and free-surface of the water as initial condition.

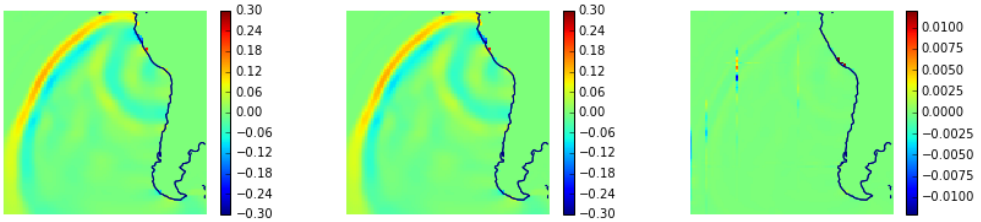

Figure 3: Comparison of the free surface elevation in the region Ω_1, for simulations using the small domain Ω_1 (left), big domain Ω_2 (center), and the difference between both of them (right), at $t = 5.75$ hours.

come from spurious reflection with the artificial boundary used in Ω_1. These differences reached a magnitude of the order of $1cm$, which can be comparable, if not with that of the leading front, possibly with secondary waves that can remain after the first arrival.

Thus, here we have shown that with the simple approach of using Neumann boundary conditions to represent open or transparent boundary conditions, some differences can be observed with respect to using a bigger domain in the simulation, and then, some improvement can be done to decrease the magnitude of these differences.

2 KdV equation

2.1 The model

The first model of wave propagation studied and implemented in this project is the Korteweg-de Bries (KdV) equation, which takes in account nonlinear and dispersive effects and is a good approximation for waves with

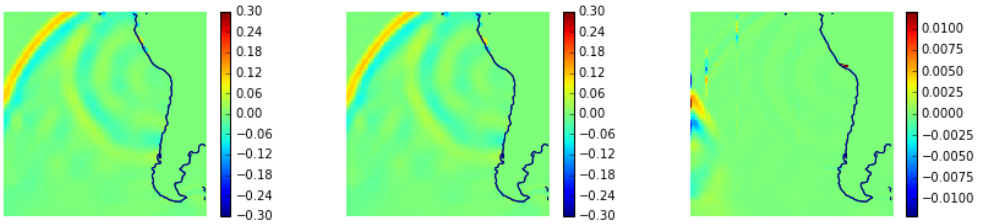

Figure 4: Comparison of the free surface elevation in the region Ω_1, for simulations using the small domain Ω_1 (left), big domain Ω_2 (center), and the difference between both of them (right), at $t = 7.00$ hours.

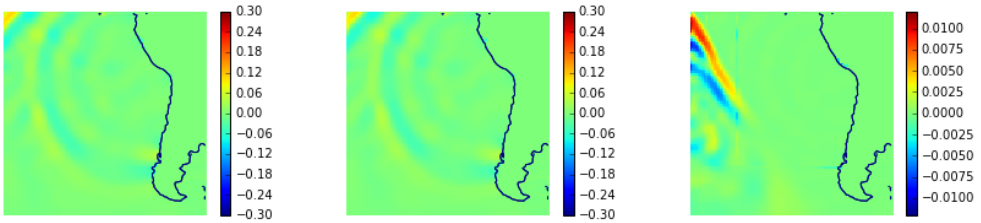

Figure 5: Comparison of the free surface elevation in the region Ω_1, for simulations using the small domain Ω_1 (left), big domain Ω_2 (center), and the difference between both of them (right), at $t = 8.75$ hours.

small amplitude and long wavelength.

Different forms of this equation can be found in literature, varying mainly in the scaling factors for each physical process present in the equation (nonlinearity and dispersion). We will consider the formulation derived by [2], written in terms of dimensionless but unscaled variables :

$$u_t + u_x + (u^2)_x + u_{xxx} = 0 \tag{1}$$

2.2 Discretization

The problem to be solved, with a initial condition Φ and proper boundary conditions, is

$$\begin{cases} u_t + u_x + (u^2)_x + u_{xxx} = 0 \ , \quad x \in [x_{min}, x_{max}], \quad t \in [0, t_{max}] \\ u(x,0) = \Phi(x) \\ + \text{ boundary conditions} \end{cases} \tag{2}$$

In a first moment, in order to validate the implementation of the model, without influence of the boundaries, we will consider periodic boundary conditions or, in the nonperiodic case, homogeneous Dirichlet and/or Neumann conditions with the boundaries far enough from the propagating wave.

The numerical resolution will be made with a splitting scheme, separating the advective and the dispersive terms. Therefore, defining the operators

$$T_a u = u_t + u_x + (u^2)_x \tag{3}$$

$$T_d u = u_t + u_{xxx} \tag{4}$$

we will solve, in each time step $[t_n, t_{n+1}]$:

$$\begin{cases} T_a(v) = 0 \ , \ t \in [t_n, t_{n+1}], \ v^n = u^n \\ T_d(w) = 0 \ , \ t \in [t_n, t_{n+1}], \ w^n = v^{n+1} \\ u^{n+1} = w^{n+1} \end{cases} \tag{5}$$

The numerical schemes used in each of these step is descried below :

2.2.1 First step

The first step of the splitted KdV equation is a hyperbolic conservation law, which can be written in terms of a flux function f :

$$v_t + f(v)_x = 0, \quad f(v) = v + v^2 \tag{6}$$

It will be solved using a Finite Volume method, with the cells $[x_{i-1/2}, x_{i+1/2}]$ centered in the discrete spatial points x_i and with the cell-averaged value of the solution equal to the solution u_i^n in these points. The spatial derivative in (6) will be discretized with a 4th order Runge-Kutta method,

$$\begin{cases} k_1 = -f(v_i^n)_x \\ k_2 = -f\left(v_i^n + k_1 \frac{\Delta t}{2}\right)_x \\ k_3 = -f\left(v_i^n + k_2 \frac{\Delta t}{2}\right)_x \\ k_4 = -f(v_i^n + k_3 \Delta t)_x \\ v_i^{n+1} = v_i^n + \frac{\Delta t}{6}(k_1 + 2k_2 + 2k_3 + k_4) \end{cases} \tag{7}$$

and the spatial derivative will be approximated in terms of the flux on the cells' interfaces :

$$f(v_i^n)_x = \frac{f\left(v_{i+1/2}^n\right) - f\left(v_{i-1/2}^n\right)}{\Delta x} \tag{8}$$

Therefore, we must compute the values of u on each interface. It will be made solving the following Riemann problem :

$$\begin{cases} v_t + f(v)_x = 0 \\ v(x,0) = v^- \ , \ x < 0 \\ v(x,0) = v^+ \ , \ x > 0 \end{cases} \tag{9}$$

where the boundary is located at $x = 0$ and v^- and v^+ are the solutions in its two neighbor cells.

The flux function f is uniformly convex, so the Riemann problem has a unique weak, admissible solution [10] :

- If $v^- > v^+$ (shock) :

$$v(x,t) = \begin{cases} v^- \ , & f(v^-) > f(v^+) \\ v^+ \ , & f(v^-) < f(v^+) \end{cases} \tag{10}$$

- If $v^+ > v^-$ (rarefaction wave) :

$$v(x,t) = \begin{cases} v^- \ , & f'(v^-) > 0 \\ (f')^{-1}(v) \ , & f'(v^-) < 0 < f'(v^+) \\ v^+ \ , & f'(v^+) < 0 \end{cases} \tag{11}$$

2.2.2 Second step

Two schemes will be proposed for the resolution of the second step of the KdV equation,

$$w_t + w_{xxx} = 0 \tag{12}$$

depending on the boundary conditions (periodic or not).

Periodic case The spatial derivatives and the linearity in the second step (12) motivates us to implement a Fourier spectral method, which is possible with the periodic boundary conditions. In fact, the method is quite simple :

Let $\hat{w}(k, t_n)$ be the Fourier coefficients of $w(x, t_n)$. The Fourier transform of the equation (12) gives

$$\hat{w}_t(k,t) - ik^3\hat{w}(k,t) = 0 \tag{13}$$

It is an ODE in t, which solution is

$$\hat{w}(k,t) = e^{ik^3(t-t_n)}\hat{w}(k,t_n) \tag{14}$$

Finally, the inverse Fourier transform using the coefficients $\hat{w}(k, t_{n+1})$ gives $w(x, t_{n+1})$

Nonperiodic case For this case, the second equation (12) was solved using an implicit Finite Difference scheme, with fourth order centered discretization of the third spatial derivative, except in the points near the boundaries, for which a simple first order uncentered scheme was used:

$$\frac{u_i^{n+1} - u_i^n}{\Delta t} + \frac{\frac{1}{8}u_{i-3}^{n+1} - u_{i-2}^{n+1} + \frac{13}{8}u_{i-1}^{n+1} - \frac{13}{8}u_{i+1}^{n+1} + u_{i+2}^{n+1} - \frac{1}{8}u_{i+3}^{n+1}}{\Delta x^3} = 0, \quad i = 3, ..., N-3 \tag{15}$$

$$\frac{u_i^{n+1} - u_i^n}{\Delta t} + \frac{-u_i^{n+1} + 3u_{i+1}^{n+1} - 3u_{i+2}^{n+1} + u_{i+3}^{n+1}}{\Delta x^3} = 0, \quad i = 0, 1, 2 \tag{16}$$

$$\frac{u_i^{n+1} - u_i^n}{\Delta t} + \frac{u_i^{n+1} - 3u_{i-1}^{n+1} + 3u_{i-2}^{n+1} - u_{i-3}^{n+1}}{\Delta x^3} = 0, \quad i = N-2, N-1, N \tag{17}$$

$$\tag{18}$$

which leads to the resolution of a linear system, with the appropriate modifications to take in account the boundary conditions.

2.2.3 Choice of the time step

The time step is chosen based on the first step of the splitted equation. In the non-conservative form, the equation (6) is written as

$$v_t + (1 + 2v)v_x = 0 \tag{19}$$

which configures an advection problem with velocity $1 + 2v$

The space and time steps must verify the CFL condition :

$$(1 + 2v)\frac{\Delta t}{\Delta x} \leq 1 \tag{20}$$

in order to avoid non-physical behaviors (e.g. mass increasing). Therefore, for each time step, we will chose, for small ε

$$\Delta t = \frac{\Delta x}{1 + 2\max\limits_{x} |v|} - \varepsilon \tag{21}$$

2.3 Scale analysis

With the objectif of correctly simulating the physical phenomena involved in the KdV equation, the initial solution must satisfy the assumptions made in the derivation of the model. Following this purpose, we perform in the next paragraphs a scale analysis following the arguments presented in [2], which at the same time will be linked to the physical case of water surface waves of small amplitude. This analysis will allow us to derive a criteria for selecting the initial conditions of some example simulations.

We will seek to write the KdV equation in the following dimensionless and scaled form, as described in [2]

$$U_T + U_X + \frac{\varepsilon}{2}(U^2)_X + \varepsilon\alpha^2 U_{XXX} = 0 \tag{22}$$

and link it to the parameters involved in the model for surface water waves in dimensional form [7]

$$u^*_{t^*} + c_0 u^*_{x^*} + \frac{3}{4}\frac{c_0}{h_0}(u^{*2})_{x^*} + \frac{1}{6}c_0 h_0^2 u^*_{x^*x^*x^*} = 0 \tag{23}$$

where the $\cdot^*$ denotes the physical variables, h_0 the undisturbed water depth for flat bottom and $c_0 = \sqrt{gh_0}$ the long wave speed.

2.3.1 Characterization of the nonlinearity

According to [2], nonlinearity is characterized by a parameter ε such that if characteristics are written in the form

$$\frac{1}{c_0}\frac{dx}{dt} = 1 + bu$$

then one can choose an $\varepsilon \ll 1$ such that $bu = \varepsilon U$, with U of order one. For the particular case of water waves this can be represented as

$$\frac{1}{c_0}\frac{dx}{dt} = 1 + \frac{3}{2h_0}u$$

and thus $b = \frac{3}{2h_0}$. This parameter will be used in the next arguments.

2.3.2 Characterization of the dispersion

The characterization of the dispersion comes from the derivation of the KdV equation. According to [2] if the propagation of the wave follows a law of the form

$$u^*_{t^*} + u^* u^*_{x^*} + (\mathcal{L}u^*)_{x^*} = 0$$

with $\mathcal{L}$ such that

$$\widehat{\mathcal{L}u^*} = \frac{c(k)}{c_0}\widehat{u^*}(k,t)$$

with $\hat{\cdot}$ the Fourier transform and $c(k)$ the phase celerity, which is equivalent to

$$\mathcal{L}u = \mathcal{F}^{-1}\left(\frac{c(k)}{c_0}\right) * u$$

where $\mathcal{F}^{-1}$ is the inverse Fourier transform operator, then new scaling based on the fact that for κ sufficiently small, the wave speed $c(\kappa) = c_0 + c_0\sum_{n=1}^{\infty} A_n \varepsilon^n \kappa^{2n}$ can be approximated by $c(\kappa) = c_0(1-\kappa^2)$, which motivates replacing $X = \sqrt{\varepsilon}x^*$, $T = c_0\sqrt{\varepsilon}t^*$, and $u^* = \frac{\varepsilon}{b}U$ to obtain the equivalent equation

$$U_T + \varepsilon U U_x + (\mathcal{L}_\varepsilon U)_X = 0$$

with $\mathcal{L}_\varepsilon$ such that

$$\widehat{\mathcal{L}_\varepsilon U} = \frac{c(\varepsilon^{1/2}K)}{c_0}\hat{U}(K,T)$$

with $K = \sqrt{\varepsilon}k$, which after replacing the full series expansion of $c(k)$ leads to

$$\mathcal{L}_\varepsilon U = U + \sum_{n=1}^{\infty}(-1)^n A_n \varepsilon^n \partial_X^{2n} U \tag{24}$$

and if terms for $n \geq 2$ are neglectable, which is the case for $\varepsilon \ll 1$ and if one supposes that all derivatives of U are of the same order of magnitude, then one obtains that

$$\begin{aligned}\mathcal{L}_\varepsilon U &= U + A_n \varepsilon \frac{\partial^2 U}{\partial x^2} \\ &= U - \alpha^2 \varepsilon \frac{\partial^2 U}{\partial x^2}\end{aligned}$$

with $\alpha^2 = -A_n$. Replacing in the scaled equation results in

$$U_T + U_X + \frac{\varepsilon}{2}(U^2)_X + \varepsilon\alpha^2 U_{XXX} = 0$$

Applying the same scaling $X = \sqrt{\varepsilon}x^*$, $T = c_0\sqrt{\varepsilon}t^*$, and $u^* = \frac{\varepsilon}{b}U$ to the physical equation leads to

$$U_T + U_X + \frac{3\varepsilon}{4h_0 b}(U^2)_X + \frac{h_0^2\varepsilon}{6}U_{XXX} = 0$$

from where, comparing to (22), one concludes that $\alpha^2 = \frac{h_0^2}{6}$

2.4 The criteria for choosing an appropriate initial solution

2.4.1 Choice of the wavelength

A sufficient condition for the terms of order greater than 1 in the power series expansion of $\mathcal{L}_\varepsilon$ (equation (24)) to be neglectable is that those terms are also neglectable for $c(k)$, given that that all the derivatives of U have an order of magnitude 1.

A key point in the derivation of the KdV equation is to assure that the terms for the higher derivatives (for $n > 1$) are small enough to be neglected. Firstly, [2] assumes that all this derivatives have have an order of magnitude

1. Secondly, a sufficient condition for this is that those terms are also neglectable in the series expansion of $c(k)$. Thirdly, also accordingly to [2], the following form is applicable to surface waves :

$$c(\kappa) = c_0 \left(\frac{tanh(\kappa h_0)}{\kappa h_0} \right) = c_0 \left(1 - \frac{1}{6}(\kappa h_0)^2 + \frac{19}{360}(\kappa h_0)^2 + ... \right)$$

from where we can see that we must choose $\kappa h_0 \ll 1$

Denoting λ as the wavelength, and choosing a constant B such that $\kappa h_0 = B \ll 1$, it follows that $h_0 = \frac{B\lambda}{2\pi}$, and, from the relation $\alpha^2 = \frac{h_0^2}{6}$, we get $\alpha^2 = \frac{B^2\lambda^2}{6(2\pi)^2}$.

2.4.2 Choice of the wave amplitude

From $bu^* = \varepsilon U$, with U of unit order magnitude, and since $b = \frac{3}{2h_0}$, the physical variable is written as $u^* = \frac{2}{3}h_0\varepsilon U$, $(\varepsilon > 0)$, thus if ε represents the amplitud of the wave, $\frac{2}{3}\varepsilon h_0$ is the wave amplitude (as done in the scale study). Accordingly to [2], the nonlinearity in the KdV equation is valid for $\varepsilon \ll 1$. Therefore, ε will be chosen taking in account this condition.

2.4.3 Resume

In resume, the proposed criteria to construct the initial data is :

1. Adopt a water depth h_0 (e.g. from the data)
2. Choose a wave amplitude $A = \frac{2}{3}h_0\varepsilon$, then the restriction $\varepsilon \ll 1$ translates to $\frac{A}{h_0} = \frac{2}{3}\varepsilon \ll 1$.
3. Choose a wavelength λ such that $\kappa h_0 = \frac{2\pi}{\lambda}h_0 = B \ll 1$, which translates to $\frac{h_0}{\lambda} = \frac{B}{2\pi} \ll 1$
4. The effect of dispersion over non linearity can be measured by taking the quotient of their coefficients $\frac{\varepsilon\alpha^2}{\varepsilon} = \alpha^2$.

From another point of view, one can define a wave of amplitude A and wavelength λ and compute the range of depths in which this initial condition is valid, for a given precision :

$$h_0^{valid} = \left[\frac{3A}{2\varepsilon}, \frac{B\lambda}{2\pi} \right] \tag{25}$$

This is consistent with the fact that the KdV model is valid for waves with small amplitude and large wavelenght [2].

2.4.4 Examples

We present here twwo examples to test the proposed numerical solution for the KdV equation. These examples are inspired in those showed in [10]: the initial solutions are gaussian waves (far enough from the boundaries in order to avoid its influence) with different amplitude and wavelength (the wavelength is adopted as the standard deviation). The idea is to verify the influence of these characteristics on the nonlinear and dispersive effects, and also to check the water depth range in which the propagation of this solution can be modeled by the KdV equation. Both tests were made with $B = 0.1$ and $\varepsilon = 0.001$.

The initial solutions used are

1. **Short wave (figure 6a)**
   - $\lambda = 1$
   - $A = 10^{-5}$
   - $h_0^{valid} = [0.15, 0.16]$
2. **Long wave (figure 6b)**
   - $\lambda = 250000$
   - $A = 0.1$
   - $h_0^{valid} = [150, 3979]$

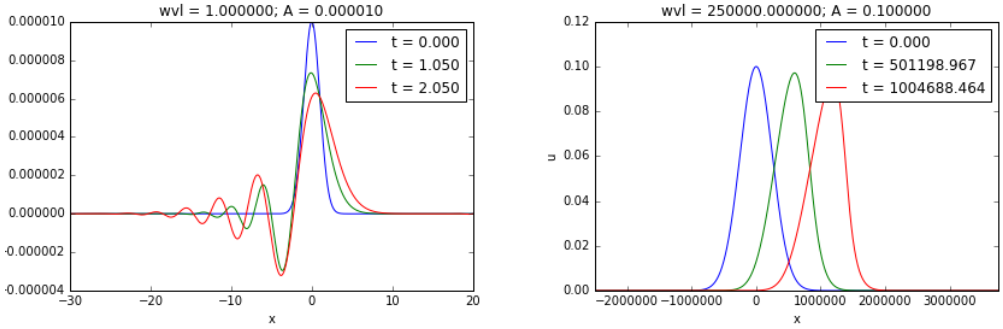

(a) Short gaussian wave

(b) Long gaussian wave

Figure 6: Simulations with the KdV equation

Conclusions :

- These results are compatible with the observations and examples made by [10], which states that dispersive effects are stronger in shorter waves; in the long wave, the nonlinear effect is more evident.
- The range of validity of the KdV equation is very small in the case of the short wave, and much larger for the long wave. This is coherent with the fact that this model is a good approximation for the propagation of long waves with small finite amplitude, which can be seen in the definition of h_0^{valid} (equation (25)) : reducing A and increasing λ increases the length of the interval of validity.
- One of our conclusions in the derivation of the proposed criteria should be revised : the one which says that the importance of the dispersive over the nonlinear effects can be measured by $\alpha^2 = \frac{h_0^2}{6}$: in fact, in the given examples, if we adopt h_0 as the median of h_0^{valid}, the highly-dispersive short wave has a smaller α^2 than the long wave.

3 BBM equation

3.1 The model

The second model for wave propagation that we consider in this project is the BBM equation, which models a long-wave propagation accounting for nonlinear and dispersive effects (in an alternative formulation for the KdV equation, with better stability and numerical properties). This equation is derived by [2] and reads

$$u_t + u_x + (u^2)_x - u_{xxt} = 0 \tag{26}$$

3.2 Discretization

The BBM model will be treated here in the same way we did for the KdV equation : we will use an split method, leading to the resolution of the following problem in each time step:

$$\begin{cases} v_t + v_x + (v^2)_x = 0 \ , \ t \in [t_n, t_{n+1}], \ v^n = u^n \\ w_t - w_{xxt} = 0 \ , \ t \in [t_n, t_{n+1}], \ w^n = v^{n+1} \\ u^{n+1} = v^{n+1} \end{cases} \tag{27}$$

given an initial solution and appropriate boundary conditions.

The first equation (which is exactly the same as in the KdV equation) will be solved with a Finite Volume method, with a 4th order Runge-Kutta discretization for the time derivative, as described in the section 2.2.1. The second equation will be solved with a Fourier spectral method in the periodic case, and a finite difference method in the nonperiodic one, as described below:

Periodic case The second equation of the BBM splitted model can be written as

$$(w - w_{xx})_t = 0$$

showing that $w - w_{xx}$ does not depend on time. Therefore, for each time step $[t_n, t_{n+1}]$:

$$w - w_{xx} = (w - w_{xx})|_{t=t_n} = (v - v_{xx})|_{t=t_{n+1}} = g(x)$$

This equation will be solved using the Fourier method. Let $\hat{w}(k, t_n)$ and $\hat{g}(k)$ be the Fourier coefficients of $w(x, t_n)$ and $g(x)$ respectively. The Fourier transform of the above equation gives

$$\hat{w}(k, t) = \frac{\hat{g}(k)}{1 + k^2}$$

The right-hand side of the last equation does not depend on time. Therefore, the inverse Fourier transform using the coefficients $\hat{w}(k, t)$ gives $w(x, t_{n+1})$.

Though the simplicity of this implementation, we did not obtained stable numerical solutions. As we moved to the study of the Serre equation, following the objectives in this project, the numerical resolution of the BBM equation remained as an open question.

Nonperiodic case We propose for the nonperiodic case a Finite Difference discretization of the equation (3.2), which is a second-order ODE, leading to the resolution of the linear system

$$Aw^{n+1} = g$$

Nevertheless, there is an evident problem with this approach. The matrix A is constructed with a Finite Difference approximation for the operator $1 - \partial_{xx}$, and, to construct the right hand side of the linear system, we must approximate $g = (v - v_{xx})|_{t=t_{n+1}}$, which is the same operator applied to $v|_{t=t_{n+1}}$. In other words, we will have a system of the form

$$Aw^{n+1} = Av^{n+1}$$

and, as A is nonsingular, we conclude that $w^{n+1} = v^n$, which means that the dispersive part of the BBM equation does not modify the solution. Evidently, this is not necessarily true if we modify the matrix in the left side of 3.2 to take in account the boundary conditions, but if we consider an example in which the domain is much larger than the support of the initial solution (as we have done for the nonperiodic test cases for the KdV equation, with solutions far enough from the boundaries), this problem is observed.

4 Serre equation

4.1 The model

The Serre equations are a model to describe highly nonlinear waves propagating in shallow waters. Considering a horizontal bottom, these equations are written as

$$h_t + (hu)_x = 0 \tag{28}$$

$$u_t + uu_x + gh_x - \frac{1}{3h}\left(h^3\left(u_{xt} + uu_{xx} - (u_x)^2\right)\right)_x = 0 \tag{29}$$

where $u = u(x,t)$, $h = h(x,t)$ and g are, respectively, the depth-averaged horizontal velocity of the fluid, the water depth and the gravity acceleration. This formulation is based on [4].

4.2 Discretization

As done previously for the numerical resolution of the KdV and the BBM equations, the Serre equations will be numerically solved using a splitting method, in which the system of equations will be decomposed in two : the first one will contain the advection terms, and the second one, all the high-order derivative terms.

Therefore, the numerical resolution will consist in solve, in each time step $[t_n, t_{n+1}]$, the following problem :

$$\begin{cases} \tilde{h}_t + \left(\tilde{h}\tilde{u}\right)_x = 0 \\ \tilde{u}_t + \tilde{u}\tilde{u}_x + g\tilde{h}_x = 0, \quad t \in [t_n, t_{n+1}], \quad (\tilde{h}, \tilde{u})(x, t_n) = (h, u)(x, t_n) \end{cases} \tag{30}$$

$$\begin{cases} \overline{h}_t = 0 \\ \overline{u}_t - \frac{1}{3\overline{h}} \left(\overline{h}^3 \left(\overline{u}_{xt} + \overline{u}\overline{u}_{xx} - (\overline{u}_x)^2 \right) \right)_x = 0, \quad t \in [t_n, t_{n+1}], \quad (\overline{h}, \overline{u})(x, t_n) = (\tilde{h}, \tilde{u})(x, t_{n+1}) \end{cases} \tag{31}$$

$$\Big\{ (h, u)(x, t_{n+1}) = (\overline{h}, \overline{u})(x, t_{n+1}) \tag{32}$$

If we denote the two systems by the operators $T_a^{\Delta t}$ and $T_d^{\Delta t}$, respectively, where the superscript indicates that the operator is performed over a time step Δt, the problem can be written as

$$(h, u)(x, t_{n+1}) = T_d^{\Delta t} \left(T_a^{\Delta t} \left((h, u)(x, t_n) \right) \right) \tag{33}$$

Some variations of the splitting scheme were also implemented. For example, inverting the order of the operators; or the method known as "Strang splitting", in which three problems are solved in each time-step :

$$(h, u)(x, t_{n+1}) = T_a^{\frac{\Delta t}{2}} \left(T_d^{\Delta t} \left(T_a^{\frac{\Delta t}{2}} (h, u)(x, t_n) \right) \right) \tag{34}$$

In the following descriptions of the resolution of the two schemes, the tilde and the overbar will be omitted for the sake of clarity.

4.2.1 First system of equations (advection step)

The first part of the Serre equation corresponds to the Non linear Shallow Water equation, that after noticing that

$$\begin{aligned} (hu)_t &= uh_t + hu_t = -u(hu)_x - h\left(uu_x + gh_x\right) \\ &= -u\left(h_x u + 2hu_x\right) - ghh_x \\ &= -\left(hu^2\right)_x - \frac{1}{2}g\left(h^2\right)_x = -\left(hu^2 + \frac{1}{2}gh^2\right)_x \end{aligned}$$

then it can be written as a conservation law of the form

$$U_t + F(U)_x = 0 \tag{35}$$

where $U = (h, hu)^T$, $F(U) = (hu, hu^2 + \frac{1}{2}gh^2)$. Weak solutions are approximated using a Finite Volume scheme, that is, after integrating the system (35) in a cell $\Omega_i = [x_i - \Delta x/2, x_i + \Delta x/2]$, and defining $\overline{U} = \frac{1}{\Delta x} \int_{\Omega_i} U(x)dx$, then the semidiscrete approximation to (35) is

$$\overline{U}_t + \frac{1}{\Delta x}\left(F(U_{i+1/2}) - F(U_{i-1/2})\right) = 0 \tag{36}$$

where $U_{i\pm 1/2}$ corresponds to the values of the conserved variables at the interface of each cell.

The values at each interface $U^* = U_{i+1/2}$ are obtained from the solution to the Riemann problem of the non-conservative form of (35) between two states $U_L = U_i$ and $U_R = U_{i+1}$

$$\begin{aligned} U_t + A(U)U_x &= 0 \\ U(t=0,x) &= \begin{cases} U_l & , \text{ if } x \leq 0. \\ U_r & , \text{ if } x > 0 \end{cases} \end{aligned} \tag{37}$$

where A is the jacobian matrix of $F(U)$. The solution to this Riemann problem is found using the approximate Riemann solver of Roe that is described in reference [8]. It consists first of a change of variables that allows to write (37) as

$$\begin{aligned} V_t + C(V)V_x &= 0 \\ V(t=0,x) &= \begin{cases} V_l & , \text{ if } x \leq 0. \\ V_r & , \text{ if } x > 0 \end{cases} \end{aligned} \tag{38}$$

with $V = (2c, u)^T$ and $C(V) = \begin{pmatrix} u & c \\ c & u \end{pmatrix}$. Second, instead of using the exact formulation, a linearized problem is solved using $C(\hat{V})$ in place of $C(V)$, with $\hat{V} = (V_L + V_R)/2$. The matrix $C(\hat{V})$ is diagonalizable and thus, a decoupled system can be obtained in the form

$$\begin{aligned} (w_1)_t + \hat{\lambda}_1(w_1)_x &= 0 \\ (w_2)_t + \hat{\lambda}_2(w_2)_x &= 0 \\ (w_1, w_2)^T(t=0,x) &= \begin{cases} ((w_1)_L, (w_2)_L)^T & , \text{ if } x \leq 0. \\ ((w_1)_L, (w_2)_L)^T & , \text{ if } x > 0 \end{cases} \end{aligned} \tag{39}$$

where $\hat{\lambda}_1 = \hat{u} - \hat{c}$, $\hat{\lambda}_2 = \hat{u} + \hat{c}$, $w_1 = u - 2c$, $w_2 = u + 2c$ and $(w_1)_L = u_L - 2c_L, (w_2)_L = u_L - 2c_L$, $(w_1)_R = u_R - 2c_R, (w_2)_R = u_R - 2c_R$. Writing $W = (w_1, w_2)$ and using index $*, L, R$, for the values at the interface, left and right states, and noticing that $\hat{\lambda}_1 \leq \hat{\lambda}_2$, the solution can be found for separate cases:

- If $\lambda_1 > 0$, then $W^* = W_L$
- If $\lambda_1 \leq 0$ and $\lambda_2 > 0$, $W^* = ((w_R)_1, (w_L)_2)^T$
- If $\lambda_2 \leq 0$, $W^* = W_R$

the values at the interface can then be recovered setting the inverse transformation

$$\begin{aligned} u^* &= \frac{1}{2}(w_1^* + w_2^*) \\ h^* &= \frac{1}{16g}(w_2^* - w_1^*)^2 \end{aligned} \tag{40}$$

A third step is necessary, which consists on an entropy fix to select only weak solutions that are physically consistent. This is simply obtained by setting $W^* = \hat{W}$ whenever $(\lambda_1)_L < 0$ and $(\lambda_1)_r > 0$, or $(\lambda_2)_L < 0$ and $(\lambda_2)_R > 0$.

Second order Finite Volume Scheme To obtain second order convergence for smooth solutions a MUSCL (Monotonic Upstream-Centered Scheme) is used. This means that instead of solving a Riemann problem between $U_L = U_i$ and $U_R = U_{i+1}$ one must solve for $U_L = U_{i+1/2^-}$ and $U_{i+1/2^+}$, where $U_{i+1/2^+} = U_i + \frac{\Delta x}{2}s$, $s = minmod(s_L, s_R)$, $s_L = \frac{U_i - U_{i-1}}{\Delta x}$, $s_R = \frac{U_{i+1} - U_i}{\Delta x}$ and

$$minmod(s_1, s_2) = \begin{cases} min(s_1, s_2) & \text{if } s_1 > 0 \text{ } and \text{ } s_2 > 0 \\ max(s_1, s_2) & \text{if } s_1 < 0 \text{ } and \text{ } s_2 < 0 \\ 0 & elsewhere \end{cases} \tag{41}$$

4.2.2 First system of equations (advection step)

In the second system (31) of the splitted Serre equations , the water depth h is constant in time, and therefore only the velocity u must be updated. Separating the terms containing time derivatives, the second equation of thi system can be rewritten as

$$\left(u - hh_x u_x - \frac{1}{3}h^2 u_{xx}\right)_t - \frac{1}{3h}\left(h^3\left(uu_{xx} - (u_x)^2\right)\right)_x = 0 \tag{42}$$

This equation will be solved using an explicit Finite Difference scheme. Defining

$$g_1 = h^3 \left(u u_{xx} - (u_x)^2 \right)$$

$$g_2 = u - h h_x u_x - \frac{1}{3} h^2 u_{xx}$$

where the derivatives are evalueated using appropriate finite difference approximations.

With this notation, using an one-step forward time discretization, one gets

$$(g_2)_i^{n+1} = (g_2)_i^n + \frac{\Delta t}{3 h_i^n} \left((g_1)_x \right)_i^n = G_i^n$$

where the superscript and the subscript denotes respectively the time step and the spatial position.

Using 2nd order centered approximation for the spatial derivatives in $(g_2)_i^{n+1}$, one gets the following tridiagonal linear system :

$$\left(\frac{h_i^n (h_x)_i^n}{2\Delta x} - \frac{(h_i^n)^2}{3\Delta x^2} \right) u_{i-1}^{n+1} + \left(1 + \frac{2(h_i^n)^2}{3\Delta x^2} \right) u_i^{n+1} + \left(-\frac{h_i^n (h_x)_i^n}{2\Delta x} - \frac{(h_i^n)^2}{3\Delta x^2} \right) u_{i+1}^{n+1} = G_i^n$$

with the appropriate modifications to take in account the boundary conditions.

Alternative formulation of the second system (for the variables (h, hu)) Inspired by the discretization described in [3], we will rewrite the second system of equations obtained in the splitting of the Serre equations, in order to solve it in the variables (h, hu) and thus keep the formulation of the first system.

The detailed derivation of this alternative formulation is described in the appendix of this rapport. Applying a splitting scheme for the obtained system, the first step remains the same (the NSWE), and the second one turns in

$$T_d := \begin{cases} h_t = 0 \\ (hu)_t - g h h_x + (I + h \mathcal{T} \frac{1}{h})^{-1} \left[g h h_x + h \mathcal{Q}_1(u) \right] = 0 \end{cases} \tag{43}$$

where the operators $\mathcal{T}$ and $\mathcal{Q}_1$ are defined as

$$\mathcal{T}(w) = -\frac{1}{3h}(h^3 w_x)_x = -\frac{h^2}{3} w_{xx} - h h_x w_x$$

$$\mathcal{Q}(w) = \frac{2}{3h}(h^3 (w_x)^2)_x = \frac{4h^2}{3}(w_x w_{xx}) + 2 h h_x (w_x)^2$$

Defining the operator

$$\tilde{\mathcal{T}} w = I + h\mathcal{T}\frac{1}{h} \tag{44}$$

we will in each time step solve the linear system

$$\left(\tilde{\mathcal{T}}\right)^{-1}\left[hh_x + h\mathcal{Q}_1(u)\right] = z \implies \tilde{\mathcal{T}} z = hh_x + h\mathcal{Q}_1(u) \tag{45}$$

The left side of (45) is

$$\begin{aligned}
&\tilde{\mathcal{T}} z = (I + h\mathcal{T}\frac{1}{h})z = \\
&\quad z - \frac{h^3}{3}\left(\frac{1}{h}z\right)_{xx} - h^2 h_x\left(\frac{1}{h}z\right)_x = \\
&\quad z - \frac{h^3}{3}\left[\left(2\frac{(h_x)^2}{h^3} - \frac{h_{xx}}{h^2}\right)z - 2\frac{h_x}{h^2}z_x + \frac{z_{xx}}{h}\right] - h^2 h_x\left[-\frac{h_x}{h^2}z + \frac{z_x}{h}\right] = \\
&\quad \left(1 + \frac{1}{3}(h_x)^2 + \frac{1}{3}hh_{xx}\right)z - \left(\frac{1}{3}hh_x\right)z_x - \left(\frac{1}{3}h^2\right)z_{xx}
\end{aligned} \tag{46}$$

Using second-order finite difference discretizations in space, we solve, for each $i = 1, ..., N-1$ in the time step t_n :

$$\begin{aligned}
\left(1 + \frac{1}{3}((h_x)_i^n)^2 + \frac{1}{3}h_i^n(h_{xx})_i^n + \frac{1}{\Delta x^2}\frac{2}{3}(h_i^n)^2\right)z_i^n + \frac{1}{3}\left(-\frac{h_i^n(h_x)_i^n}{2\Delta x} - \frac{(h_i^n)^2}{\Delta x^2}\right)z_{i+1}^n + \\
\frac{1}{3}\left(\frac{h_i^n(h_x)_i^n}{2\Delta x} - \frac{(h_i^n)^2}{\Delta x^2}\right)z_{i-1}^n = \\
h_i^n(h_x)_i^n + h_i^n(\mathcal{Q}_1(u))_i^n
\end{aligned} \tag{47}$$

Therefore, for each $i = 1, ...N-1$, the actualization of the solution in time is given by

$$(hu)_i^{n+1} = (hu)_i^n + \Delta t\left(gh_i^n(h_x)_i^n - z_i^n\right) \tag{48}$$

4.3 Simulations

4.3.1 Description of the initial solution

In order to validate the implementation of the Serre equations, we will solve it using as initial solution the analytical solution. According to [4], the Serre equations admit the following family of periodic solutions

$$h(x,t) = a_0 + a_1 dn^2(\kappa(x-ct),k)$$
$$u(x,t) = c\left(1 - \frac{h_0}{h(x,t)}\right)$$

$$\kappa = \frac{\sqrt{3a_1}}{2\sqrt{a_0(a_0+a_1)(a_0+(1-k^2)a_1)}}$$
$$c = \frac{\sqrt{ga_0(a_0+a_1)(a_0+(1-k^2)a_1)}}{h_0}$$

with $k \in (0,1)$, $a_0 > 0$ and $a_1 > 0$, $dn(\cdot,k)$ is a Jacobi elliptic function with elliptic modulus k.

The relation between the wavelength λ and $k \in (0,1)$ is

$$\lambda = \frac{2K(k)}{\kappa}$$

and the mean water depth, h_0 is computed as

$$h_0 = \frac{1}{\lambda}\int_0^{\lambda} h(x,t)dx = a_0 + a_1\frac{E(k)}{K(k)}$$

with $K(k)$ and $E(k)$ are the complete elliptic integrals of the first and second kinds.

The limit for $k \to 0^+$ is constant water level $a_0 + a_1$ at rest. If $k \to 1^-$ it converges to the Rayleigh solitary wave solution. We will also test this last case, in which the solution is described by

$$h(x,t) = a_0 + a_1 sech^2(\kappa(x-ct),k)$$
$$u(x,t) = c\left(1 - \frac{a_0}{h(x,t)}\right)$$

$$\kappa = \frac{\sqrt{3a_1}}{2\sqrt{a_0(a_0+a_1)}}$$
$$c = \sqrt{ga_0(a_0+a_1)}$$

The expressions for the wavelength λ and the mean water depth h_0 are the same as shown for the general case of the cnoidal solution.

4.3.2 Results

With the objective to observe the nonlinear and the dispersive processes in the model, we solved the Serre equation and the Nonlinear Shallow Water Equation (NSWE), which is the first step of the proposed split scheme. The figures 7 and 8 shows the evolution of (h, u) for the cnoidal solution; and the figures 9 and 10 for the solitary solution. In this last case, we also solved the problem with a first order finite volume solver for the resolution of the first step of the Serre equation.

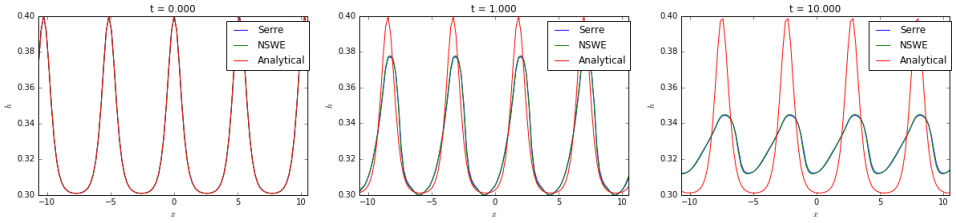

Figure 7: Evolution of h for the cnoidal solution in the Serre equation. Comparison between the analytical solution (in red) and the solutions (practically overlapped) computed with the Serre (in blue) and the NSWE (in green) models

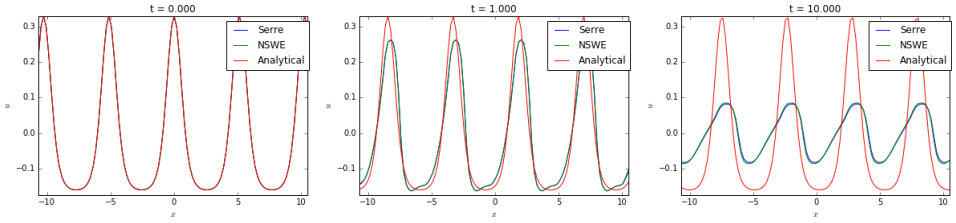

Figure 8: Evolution of u for the cnoidal solution. Comparison between the analytical solution (in red) and the solutions (practically overlapped) computed with the Serre (in blue) and the NSWE (in green) models

The results show the existence of modeling or programming errors. In both cases tested, the analytical solution is not preserved : we observe a strong dissipation of the solution, and, in the solitary wave case, an inversion of the velocity that causes the formation of secondary waves. The utilization of a higher-order solver for the Finite Volume scheme did not correct this last problem, but showed a lower dissipation.

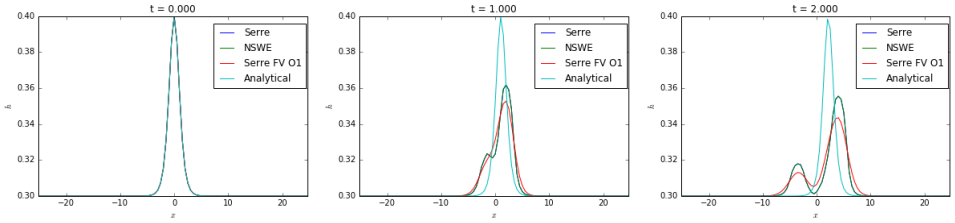

Figure 9: Evolution of h for the solitary solution. Comparison between the analytical solution (in light blue) and the solutions computed with the Serre model with first order resolution for the finite volume scheme (in red), the Serre model with second order resolution for the finite volume scheme (in dark blue) and the second order NSWE model (in green). The last two solutions are practically overlapped

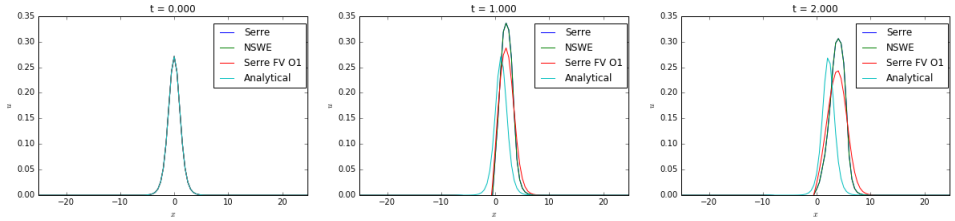

Figure 10: Evolution of u for the solitary solution. Comparison between the analytical solution (in light blue) and the solutions computed with the Serre model with first order resolution for the finite volume scheme (in red), the Serre model with second order resolution for the finite volume scheme (in dark blue) and the second order NSWE model (in green). The last two solutions are practically overlapped

5 Study of transparent boundary conditions

5.1 Introduction and motivational examples

The work presented in this section is an introduction to the objectives that we are looking for in this project, concerning the study of Transparent Boundary Conditions (TBCs). It was developed on the KdV equation, because, among the models studied and implement until here (KdV, BBM and Serre equations), it was the one for which we have obtained the best computational implementation.

The TBCs are constructed such that the solution computed in the finite computational domain Ω coincides with the solution of the whole-space problem, restricted to Ω . In general, these boundary conditions are nonlocal in time, so they must be approximated for an efficient numerical implementation [1]. Before moving to the models of wave propagation, in order to see in practice this definition we will implement a simple example, with analytical solution and TBCs, derived following [6]. We will consider the 1D problem

$$\begin{cases} -u''(x) = 1 \;\; in \;\; \Omega = [0,2] \\ u(0) = 0 \\ u(2) = 0 \end{cases} \tag{49}$$

whose solution is

$$u(x) = -\frac{x^2}{2} + x$$

and, considering the partition of Ω in $\Omega_1 = [0,1]$ and $\Omega_2 = [1,2]$, we will solve the problem

$$\begin{cases} -u_1''(x) = 1 \;\; in \;\; \Omega_1 \\ u_1(0) = 0 \\ B(u_1) = 0 \;\; at \;\; \Gamma = \{1\} \end{cases} \tag{50}$$

where the transparent boundary condition $B(u)$ is such that $u|_{\Omega_1} = u_1$.

The TBC is written in the form $B(u) = \frac{\partial}{\partial x}u + D2N(u)$, where the D2N (Dirichlet to Neumann) operator is defined by

$$D2N : \alpha(x) \mapsto \left.\frac{\partial}{\partial x}v\right|_\Gamma$$

where α is defined in the boundary Γ. In the case treated here, Γ is a point, and therefore α is a scalar.

The function v is solution of

$$\begin{cases} -v''(x) = 1 \;\; in \;\; \Omega_2 \\ v(2) = 0 \\ v(1) = \alpha \;\; at \;\; \Gamma = \{1\} \end{cases} \tag{51}$$

so

$$v(x) = -\frac{x^2}{2} + \left(\frac{3}{2} - \alpha\right) + 2\alpha - 1$$

and

$$\left.\frac{\partial}{\partial x}v\right|_{x=1} = \frac{1}{2} - \alpha$$

Finally, the TBC reads

$$B(u_1) = \frac{\partial}{\partial x}u_1 + D2N(u_1) = \frac{\partial}{\partial x}u_1 + \frac{1}{2} - u_1$$

The problem was solved with a finite difference method, with centered second-order approximation for the spatial derivative, for two different grids. The figure 11 shows that the constructed TBC effectively provides a convergent solution.

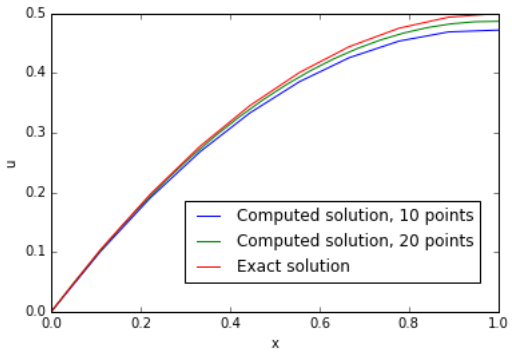

Figure 11: Solutions for the Laplace equation with TBC

Coming back to the wave models, we recall that, in the first simulations with the splitting method adopted to the resolution of the KdV equation, we did not make a rigorous application of appropriate boundary conditions. In fact, our initial objective was to validate the method; therefore, imposing periodic or homogeneous Dirichlet and Neumann conditions, we analyzed the evolution of the solution only before the arrival of the wave to the boundaries.

The following example shows very clearly the influence of inappropriate boundary conditions on the solution. We solved two times the same problem, with the same initial solution, boundary conditions, and spatial and time discretizations:

$$\begin{cases} u_t + u_x + (u^2)_x + u_{xxx} = 0 \ , \quad x \in \Omega = [a,b] \quad t \in [0, t_{max}] \\ u(x,0) = \Phi(x) \\ u(a,t) = 0 \\ u(b,t) = 0 \\ u_x(b,t) = 0 \end{cases} \tag{52}$$

The only difference is the size of the domain of each problem : they were chosen such that the wave reaches the boundaries (within the maximal time of simulation) in the first problem, but not in the second. The difference between the solution increases with the time, beginning in the boundary and propagating to the whole domain :

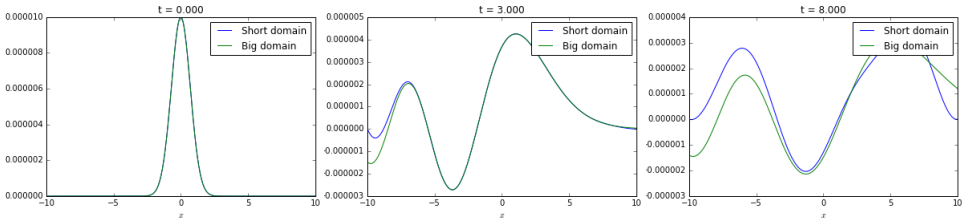

Figure 12: First motivational example : comparison between the solutions in a small and a big domain

Therefore, we look for boundaries conditions that can efficiently simulate the called Transparent Boundary Conditions (TBCs), i.e., in a such a way that the solution calculated in the computational domain Ω coincides with solution of the whole-space restricted to Ω. As a consequence, we want the boundaries not to have an influence on the solution, so, when the wave reaches the boundary, it will simply "exit" the domain. The following example shows another motivation for this work.

We want to solve the following problem :

$$(P_1)\begin{cases} u_t + u_x + (u^2)_x + u_{xxx} = 0\ , \quad x \in \Omega_1 = [0, L], \quad t \in [0, t_{max}] \\ u(x,0) = \Phi(x) \\ u(0,t) = 0 \\ u_x(0,t) = 0 \\ u(L,t) = g(t) \end{cases} \tag{53}$$

We seek a function $g(t)$ to simulate the TBC. In order to do this, we will solve before the problem

$$(P_2)\begin{cases} u_t + u_x + (u^2)_x + u_{xxx} = 0\ , \quad x \in \Omega_2 = [0, 2L], \quad t \in [0, t_{max}] \\ u(x,0) = \Phi(x) \\ u(0,t) = 0 \\ u_x(0,t) = 0 \\ u(2L,t) = 0 \end{cases} \tag{54}$$

and we impose $g(t) = u_2(t)$, where u_2 is the solution of (P_2). To obtain more precise results, the two computations are made with the same mesh size and time step.

Suppose that there is a unique solution u_1 to (P_1). We can easily see that $u_2|_{\Omega_1}$ is also a solution of (P_1). Therefore, $u_1 = u_2|_{\Omega_1}$. It justifies why our

procedure works as a TBC, as shown in the figure 13 (close-up in the region close to the right boundary) :

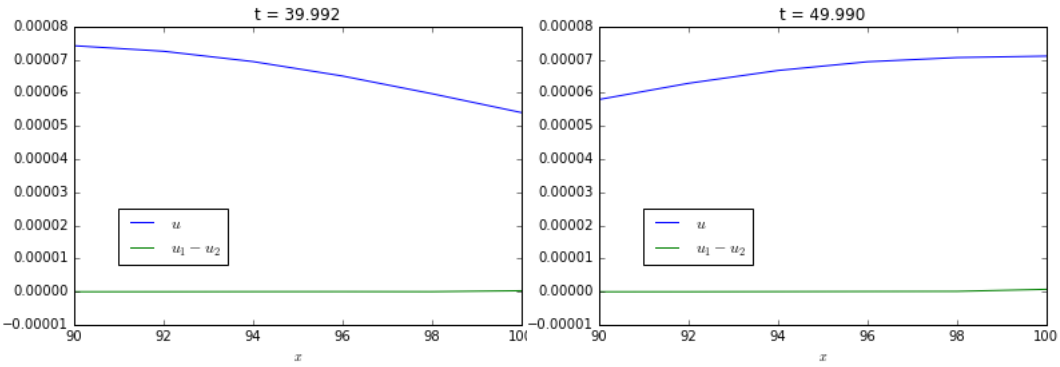

Figure 13: Second motivational example : solution with an "exact" Dirichlet condition at the right boundary

5.2 Optimization of Robin boundary conditions to simulate TBCs

5.2.1 Robin boundary conditions up to the first derivative

Although the motivating result presented in the above example, we cannot apply this procedure in practice. In fact, computing the solution in a larger domain and using it as exact solution is only a trick, which has no practical interest. Therefore, we want to determinate approximations for a TBC without having a referential solution.

The KdV will be solved in the domain $[-L, L]$ with the following boundary conditions (imposed in the resolution of the second equation of the split method):

$$\begin{cases} u(-L) = 0 \\ u_x(-L) = 0 \\ \alpha u(L) + \beta u_x(L) = 0, \quad \alpha, \beta > 0 \end{cases} \tag{55}$$

In the third condition, called a Robin boundary condition, the parameters α and β (or, equivalently, the parameter β/α) will be optimized in order to simulate a TBC. In a first moment, we will consider Robin BCs up to the first derivative of the solution.

To find the optimal coefficients, we will test several pairs $(1, \beta/\alpha)$ (including the limits $\beta/\alpha \to 0$ and $\beta/\alpha \to \infty$, corresponding respectively to

Dirichlet and Neumann BCs) and compute the error regarding to a referential solution u_{ref}, computed in a domain $[-2L, 2L]$. Two errors will be computed, for each time step t_n :

$$e_1^n = \sqrt{\sum_{i=0}^{N} (u_i^n - (u_{ref})_i^n)^2} \tag{56}$$

$$e_2^n = u_N^n - (u_{ref})_N^n \tag{57}$$

e_2^n is computed in order to show that most part of the error e_1^n of the entire domain occurs in the boundary.

The figures 14 to 17 show some snapshots and the evolution of e_1 and e_2 for some values of β/α . The figure 18 compares e_2 for many other values, including the pure Dirichlet (with $\alpha = 1, \beta = 0$, so $log(\beta/\alpha) = -\infty$) and pure Neumann (with $\alpha = 0, \beta = 1$) conditions.

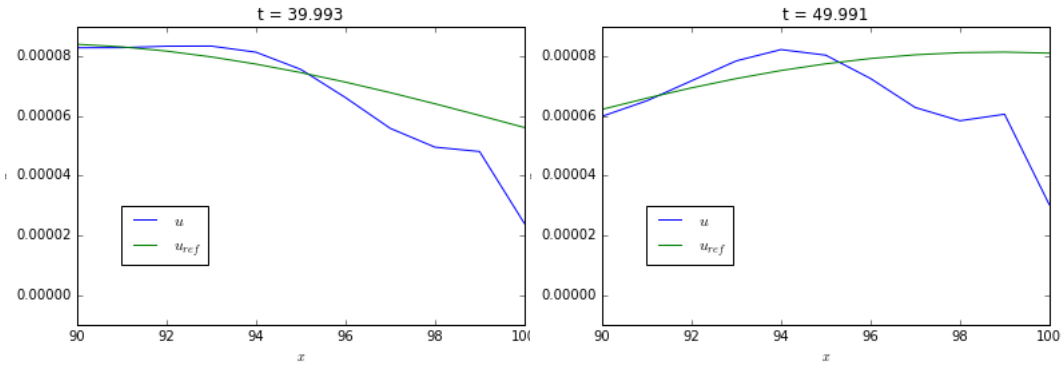

Figure 14: Computed and the referential solution for $\beta/\alpha = 1$

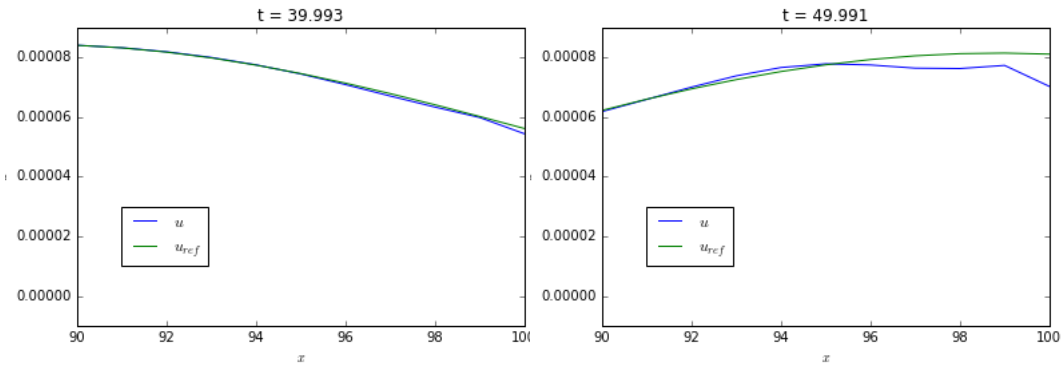

Figure 15: Computed and the referential solution for $\beta/\alpha = 10$

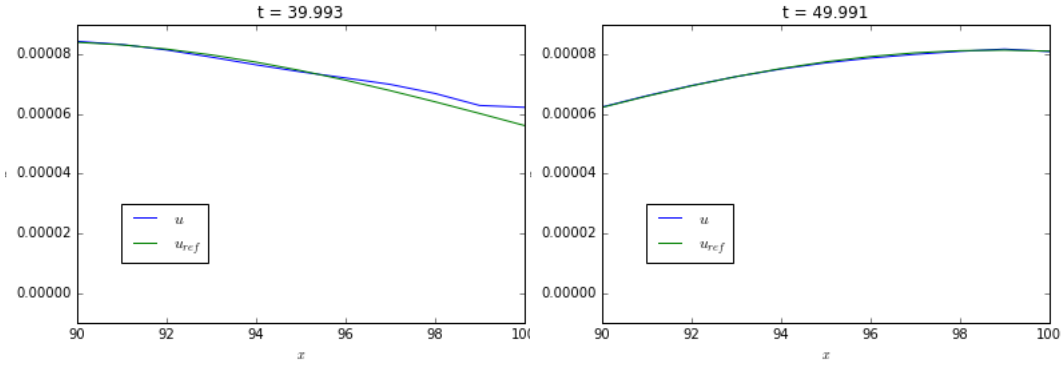

Figure 16: Computed and the referential solution for $\beta/\alpha = 100$

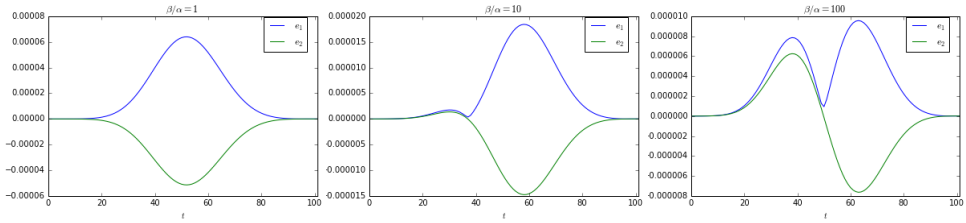

(a) $\beta/\alpha = 1$ (b) $\beta/\alpha = 10$ (c) $\beta/\alpha = 100$

Figure 17: Errors between the computed and the referential solution

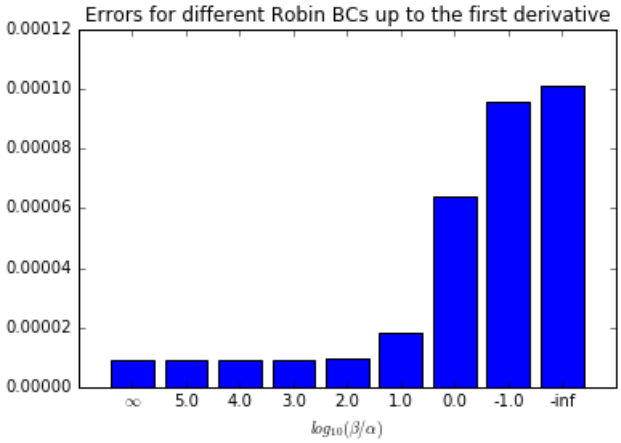

Figure 18: Error $||e_1| = \sum_{n=0}^{n_{max}} (e_1^n)^2$ between the computed and the referential solution for many values of β/α

The results presented in the figures 14 to 18 show that boundary conditions with stronger Neumann character produce better approximations to the TBC, compared to more Dirichlet-type conditions. The results for pure Neumann conditions and for Neumann with a small but non-zero Dirichlet

were very close, as presented in the table 2 for a more refined study around the best values of β/α. In fact, setting the solution to zero in the boundary is a too much strong condition, and the Neumann condition captures in a more satisfactory way the smoothness of the propagating wave.

$log(\beta/\alpha)$	Error ($\times 10^{-6}$)
2.5	8.93
3.0	8.87
3.5	8.95
4.0	8.98
4.5	8.99
5.0	8.99
∞	8.99

Table 2: Error $||e_1| = \sum_{n=0}^{n_{max}} (e_1^n)^2$ for some values of $\beta/alpha$ around the best ones

5.2.2 Robin boundary conditions up to the second derivative

We repeated the tests described above, but replacing the boundary condition in the right boundary by $\alpha u(L) + \beta u_x(L) + \gamma u_{xx}(L) = 0, \quad \alpha, \beta, \gamma > 0$.

The values of α and β will be fixed and equal to the ones that gave the minimal error in the previous simulations ($(\alpha, \beta) = (1, 1000)$). We will show directly the graph containing the errors for many values of γ/β (figure 19, which should be compared with the figure 18. Similarly to the previous conclusions, we observe a better approximation of the TBCs for stronger values of γ/β (being the error almost constant above a certain value, as show in the table 3). In fact, even the worst error in the figure 19 ($||e_1|(\gamma/\beta = 0.01) = 8.78 \times 10^{-6}$) is smaller than the best one of the table 2.

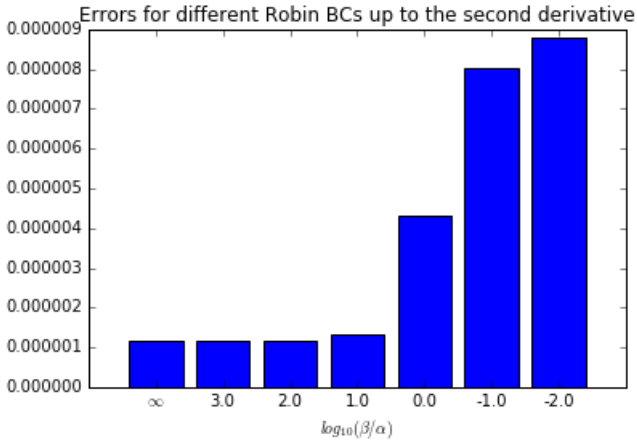

Figure 19: Error $||e_1| = \sum_{n=0}^{n_{max}} (e_1^n)^2$between the computed and the referential solution for many values of γ/β, with Robin conditions up to the second derivative

$log(\gamma/\beta)$	Error ($\times 10^{-6}$)
2.0	1.157665
2.5	1.157382
3.0	1.157280
3.5	1.157247
4.0	1.157236
4.5	1.157233
∞	1.157231

Table 3: Error $||e_1| = \sum_{n=0}^{n_{max}} (e_1^n)^2$ for some values of $\gamma/beta$ around the best ones

5.2.3 Partial conclusion

Resuming this first study of the Transparent Boundary Conditions, we looked for approximating them by Robin boundary conditions, written in a generic way, with modifiable coefficients for each term (the functions and its derivatives). The idea was to test many combinations of coefficients in order to optimize them (comparing the computed solution in $[-L, L]$ with a referential solution computed in $[-2L, 2L]$). As described above, Robin conditions taking in account the continuity of the tested function (i.e., with higher coefficients for the derivative terms) produced better results. Therefore, a TBC based on the first derivative was better than one based only on the solution; and a TBC based on the second derivative was even better. Finally, we observed that, in general, the improvement of the solution is neglectable above a certain relation between the coefficients.

6 Conclusions and next steps

Considering the work done until here and presented in this report, we can point out some further steps and problems to be solved for the continuity of the project.

Concerning the study and implementation of the models for wave propagation, we will mainly focus in the Serre equations. Our first objective is to have a reliable code to its resolution, validating it to a periodic analytical solution and after moving to different types boundary conditions. We will therefore debug the numerical implementation and review the modeling. Possible increasing of the order of the schemes used may be necessary. This work is essential for the future study of Transparent Boundary Conditions applied to the Serre equations.

In parallel, we will continue the study of TBCs. We will initially search in the literature the theory for the derivation of these conditions and the approximations that can be made to its numerical implementation. We will also continue proposing and optimizing approximations for the TBCs, in a similar as we did with the Robin boundary conditions.

7 Appendix : Equivalence between Green-Naghdi and Serre equations (in original and modified versions)

In this section, we seek to show the Green-Naghdi equations (2D) and the Serre equations (1D), written both in the variables (h, u) or (h, hu) $((h, V) or (h, hV)$ in the case of the Green-Naghdi equations).

We have initially the following equations :

- Serre equations in the variables (h, hu) :

$$\begin{cases} h_t + (hu)_x = 0 \\ u_t + uu_x + h_x - \frac{1}{3h}\left(h^3\left(u_{xt} + uu_{xx} - (u_x)^2\right)\right)_x = 0 \end{cases} \tag{58}$$

- Green-Naghdi equations in the variables (h, V) :

$$\begin{cases} h_t + \nabla \cdot (hV) = 0 \\ (I + \mathcal{T})V_t + (I + \mathcal{T})(V \cdot \nabla)V + g\nabla h + \mathcal{Q}_1(V) = 0 \end{cases} \tag{59}$$

- Green-Naghdi equations in the variables (h, hV) :

$$\begin{cases} h_t + \nabla \cdot (hV) = 0 \\ (I + h\mathcal{T}\frac{1}{h})(hV)_t + (I + h\mathcal{T}\frac{1}{h})\nabla \cdot (hV \otimes V) + gh\nabla h + h\mathcal{Q}_1(V) = 0 \end{cases} \tag{60}$$

The equation (58) is the one presented in [4] and used in this project; the equation (59) is presented in [3], in which the equation (60) is derived. Finally, the equations presented in these references were rewritten in the dimensional version and considering a flat bottom.

Also considering these simplifications, the operators $\mathcal{T}$ and $\mathcal{Q}_1$ are defined by [3] :

$$\mathcal{T}(w) = -\frac{1}{3h}\nabla(h^3\nabla\cdot w) \tag{61}$$

$$\mathcal{Q}_1(w) = \frac{2}{3h}\nabla(h^3(\nabla\cdot w)^2) \tag{62}$$

In one dimension, also as presented by [3], (61) and (62) are written as

$$\mathcal{T}(w) = -\frac{1}{3h}(h^3 w_x)_x = -\frac{h^2}{3}w_{xx} - hh_x w_x \tag{63}$$

$$\mathcal{Q}(w) = \frac{2}{3h}(h^3(w_x)^2)_x = \frac{4h^2}{3}(w_x w_{xx}) + 2hh_x(w_x)^2 \tag{64}$$

Firstly, we will obtain (58) from (59) considering the 1D case. Secondly, we will rewrite (60) also in the 1D case. Thirdly, we will rewrite (58) in the variables (h, hu) following the steps of the derivation of (60) from (59), as presented in [3]. These transformations are evident in the case of the first equation of these systems, so will only work on the second equations.

7.0.1 Derivation of the equation (58) from (59)

Writing (59) in one dimension, we have

$$\begin{aligned}
(1+\mathcal{T})u_t + (1+\mathcal{T})uu_x + h_x + Q_1(u) &= 0 \\
\implies u_t - \frac{1}{3h}(h^3(u_t)_x)_x + uu_x - \frac{1}{3h}(h^3(uu_x)_x)_x + gh_x + \frac{2}{3h}(h^3((u_t)_x)^2)_x &= 0 \\
\implies u_t - \frac{1}{3h}(h^3 u_{xt})_x + uu_x - \frac{1}{3h}(h^3((u_x)^2 + uu_{xx}))_x + gh_x + \frac{1}{3h}(2h^3(u_x)^2)_x &= 0 \\
\implies u_t + uu_x + gh_x - \frac{1}{3h}\left(h^3\left(u_{xt} + uu_{xx} - (u_x)^2\right)\right)_x &= 0
\end{aligned} \tag{65}$$

so we have obtained the 1D serre equations in the variables (h, u) (equation (58))

7.0.2 Derivation of the 1D version of (60)

In a similar way :

$$
\begin{aligned}
(I + h\mathcal{T}\frac{1}{h})(hu)_t + (I + h\mathcal{T}\frac{1}{h})(hu^2)_x + ghh_x + h\mathcal{Q}_1(u) = 0 \\
\implies (hu)_t - \frac{1}{3}\left[h^3\left(\frac{1}{h}(hu)_t\right)_x\right]_x + (hu^2)_x - \frac{1}{3}\left[h^3\left(\frac{1}{h}(hu^2)_x\right)_x\right]_x + \\
ghh_x + \frac{2}{3}(h^3(u_x)^2)_x = 0 \\
\implies (hu)_t + (hu^2)_x + ghh_x - \frac{1}{3}\left[h^3\left(\left(\frac{1}{h}(hu)_t\right)_x + \left(\frac{1}{h}(hu^2)_x\right)_x - 2(u_x)^2\right)\right]_x = 0
\end{aligned} \tag{66}
$$

For the numerical resolution of this equation, [3] presents it in terms of the inverse operator $(I + h\mathcal{T}\frac{1}{h})^{-1}$. Moreover, in order to improve the dispersive properties of the equation, a coefficient α is used, introducing in the equation (66) the terms $\frac{\alpha-1}{\alpha}(I+h\mathcal{T}\frac{1}{h})hh_x+\frac{1}{\alpha}hh_x$. Considering these remarks, the final implemented system of equations is

$$
\begin{cases}
h_t + (hu)_x = 0 \\
(hu)_t + (hu^2)_x + \frac{\alpha-1}{\alpha}ghh_x + (I + h\mathcal{T}\frac{1}{h})^{-1}\left[\frac{1}{\alpha}gh_hx + h\mathcal{Q}_1(u)\right] = 0
\end{cases} \tag{67}
$$

We remark that $\alpha = 1$ recovers the original Green-Naghdi model (which correspond to the case treated in this project).

Finally, [3] solves 67 with a splitting scheme, defining an operator with the advective terms (which corresponds to the NSWE) and another with the dispersive terms :

$$
T_a := \begin{cases}
h_t + (hu)_x = 0 \\
(hu)_t + (hu^2)_x + ghh_x = 0
\end{cases} \tag{68}
$$

$$
T_d := \begin{cases}
h_t = 0 \\
(hu)_t - \frac{1}{\alpha}ghh_x + (I + h\mathcal{T}\frac{1}{h})^{-1}\left[\frac{1}{\alpha}ghh_x + h\mathcal{Q}_1(u)\right] = 0
\end{cases} \tag{69}
$$

7.1 Reformulation of the Serre equations 58 in the variables (h, hu)

We will follow the procedure used in [3] for obtaining (60) from (59). We will use the the identities

$$
(hu^2)_x = (huu)_x = (hu)_x u + huu_x \tag{70}
$$

and

$$hu_t = (hu)_t - h_t u = (hu)_t + (hu)_x u \tag{71}$$

which derives from the first equation of the Serre model (58).

Multiplying (58) by h, we get

$$\begin{aligned} hu_t + huu_x + ghh_x - \frac{1}{3}\left(h^3\left(u_{xt} + uu_{xx} - (u_x)^2\right)\right)_x = 0 \\ \implies (hu)_t + (hu)_x u + (hu^2)_x - (hu)_x u + ghh_x - \frac{1}{3}\left(h^3\left(u_{xt} + uu_{xx} - (u_x)^2\right)\right)_x = 0 \\ \implies (hu)_t + (hu^2)_x + ghh_x - \frac{1}{3}\left(h^3\left(u_{xt} + (uu_x)_x - (u_x)^2\right)\right)_x = 0 \end{aligned} \tag{72}$$

We notice that

$$\begin{aligned} u_{xt} = \left(\frac{1}{h}(hu)\right)_{xt} = \left(-\frac{h_t}{h^2}(hu) + \frac{1}{h}(hu)_t\right)_x = \left(-\frac{h_t u}{h} + \frac{1}{h}(hu)_t\right)_x = \\ \left(\frac{1}{h}(hu)_x u)\right)_x + \left(\frac{1}{h}(hu)_t\right)_x = 0 \end{aligned} \tag{73}$$

and

$$(uu_x)_x = \left(\frac{1}{h}(huu_x)\right)_x = \left(\frac{1}{h}((hu^2)_x - (hu)_x u)\right)_x = \left(\frac{1}{h}(hu^2)_x\right)_x - \left(\frac{1}{h}(hu)_x u\right)_x \tag{74}$$

so, in (72), we obtain

$$(hu)_t + (hu^2)_x + ghh_x - \frac{1}{3}\left[h^3\left(\left(\frac{1}{h}(hu)_t\right)_x + \left(\frac{1}{h}(hu^2)_x\right)_x - 2(u_x)^2\right)\right]_x = 0 \tag{75}$$

which is the same equation that we obtained in (66). Therefore, we can write (75) as

$$(I + h\mathcal{T}\frac{1}{h})(hu)_t + (I + h\mathcal{T}\frac{1}{h})(hu^2)_x + ghh_x + h\mathcal{Q}_1(u) + ghh_x - ghh_x = 0 \tag{76}$$

where the term ghh_x was added and subtracted in order to obtain an equation in the same form of (67) (in which the coefficient α not necessarily equal to 1 causes the existence of these additional terms).

Finally, using a splitting method, we recover the systems implemented by [3] :

$$T_a := \begin{cases} h_t + (hu)_x = 0 \\ (hu)_t + (hu^2)_x + ghh_x = 0 \end{cases} \tag{77}$$

$$T_d := \begin{cases} h_t = 0 \\ (hu)_t - ghh_x + (I + h\mathcal{T}\frac{1}{h})^{-1}\left[ghh_x + h\mathcal{Q}_1(u)\right] = 0 \end{cases} \tag{78}$$

References

[1] X. Antoine, A. Arnold, C. Besse, M. Ehrhardt, and C. Schädle. A review of Transparent Boundary Conditions or linear and nonlinear Schrödinger equations. *Communications in Compuational Physics*, 4(4):729–796, October 2008.

[2] T. B. Benjamin, J. L. Bona, and J. J. Mahony. Model equations for long waves in nonlinear dispersive systems. *Philosophical Transactions of the Royal Society of London. Series A, Mathematical and Physical Sciences*, 272(1220):47–78, 1972.

[3] P. Bonneton, F. Chazel, D. Lannes, F. Marche, and M. Tissier. A Splitting approach for the fully nonlinear and weakly dispersive Green-Naghdi model. *J. Comput. Phys.*, 230:1479–1498, 2011.

[4] J. D. Carter and R. Cienfuegos. The kinematics and stability of solitary and cnoidal wave solutions of the Serre equations. *European Journal of Mechanics B/Fluids*, 2011.

[5] Clawpack Development Team. Clawpack software, 2014. Version x.y.

[6] C. Japhet and F. Nataf. The best interface conditions for Domain Decompostion methods : Absorbing Boundary Conditions. http://www.ann.jussieu.fr/ nataf/chapitre.pdf.

[7] Z. Khorsand and H. Kalisch. On the shoaling of solitary waves in the kdv equation. *Coastal Engineering Proceedings*, 1(34):44, 2014.

[8] F. Marche, P. Bonneton, P. Fabric, and N. Seguin. Evaluation of well-balanced bore-capturing schemes for 2d wetting and drying processes. *International Journal for Numerical Methods in Fluids*, 53:867–894, 2006.

[9] Y. Okada. Surface deformation due to shear and tensile faults in a half-space. *Bulletin of the seismological society of America*, 75(4):1135–1154, 1985.

[10] University of Stanford. Partial differential equations of applied mathematics - lecture 3 : Conservation laws. http://web.stanford.edu/class/math220a/handouts/conservation.pdf, 2002.